

RESEARCH NOTES FROM COLLABORATIONS

Small scintillating cells as the active elements in a digital hadron calorimeter for the e^+e^- linear collider detector

A Dyshkant, D Beznosko, G Blazey, D Chakraborty, K Francis, D Kubik, J G Lima, M I Martin, J McCormick, V Rykalin and V Zutshi

Department of Physics, Northern Illinois University, DeKalb, IL 60115, USA

E-mail: dyshkant@fnal.gov

Received 19 February 2004

Published 2 August 2004

Online at stacks.iop.org/JPhysG/30/N1

doi:10.1088/0954-3899/30/9/N01

Abstract

The ability to distinguish between hadronic W and Z decays is one of the most challenging requirements for the future linear collider detector. Such sensitivity requires unprecedented jet energy resolution, which may be possible with energy-flow algorithms. A calorimeter that is optimized for energy-flow must have fine lateral and longitudinal segmentation. Small scintillating cells with wavelength shifting fibre readout represent an attractive basis for a digital hadron calorimeter that trades dynamic range for superior granularity, at an affordable price. We present the expected jet resolution for such a device, based on Monte Carlo simulations. Then we describe the initial prototyping studies. In particular, detailed studies are presented on cell performance under different combinations of manufacture and assembly.

(Some figures in this article are in colour only in the electronic version)

1. Introduction

The current Tevatron run at Fermi National Accelerator Laboratory and the anticipated operation of the large hadron collider (LHC) at CERN are clear priorities for the present and immediate future of the high-energy physics frontier. Simultaneously, preparation for the next step, a linear electron–positron collider (LC) [1], has begun. A comprehensive feasibility study for a scintillator sampling hadron calorimeter for the LC is underway at the Northern Illinois Center for Accelerator and Detector Development (NICADD). In this note we report on the preliminary prototyping studies of a digital hadron calorimeter (DHC) constructed with small scintillating cells with optical readout. Section 2 presents a short description of a plausible hadron calorimeter configuration for a linear collider detector (LCD) system.

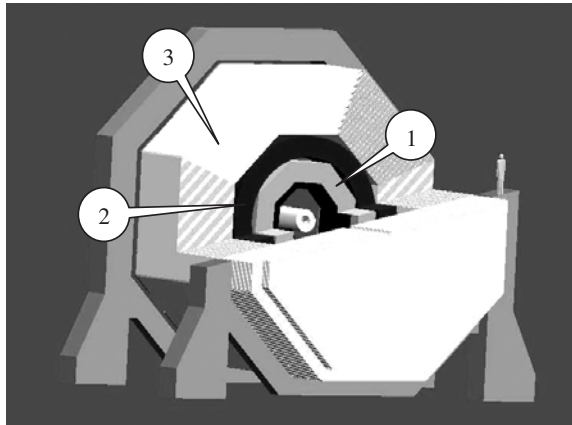


Figure 1. Schematic view of the proposed LCD [1]: 1—hadronic calorimeter, 2—magnetic coil, 3—muon system.

Section 3 compares the analog and digital approaches for a scintillating hadron calorimeter. The main results regarding the tests of cell composition, shape and construction are presented in section 4. Conclusions are given in section 5.

2. DHC for the linear collider detector

In the proposed LCD [1] (figure 1), the barrel of the sampling hadron calorimeter is ~ 1 m deep with a length of ~ 6 m. The inner radius of this calorimeter depends on the tracker option (silicon or gas) chosen. The entire device is immersed in a 5 T magnetic field. We propose to use 5 mm thick, small scintillating cells with the areas of 4–10 cm² as the primary elements of the active medium.

The cells will be connected to photo-detectors via wavelength shifting (WLS) fibres either inside the magnetic field, or outside it with additional clear fibre. This type of calorimeter will consequently have a large number of independent channels with fast readout and good time resolution to avoid event pile-up. Because the average occupancy per cell will be much less than 1, the readout can be reduced to a single threshold (or bit) that detects the passage of a minimum ionizing particle (MIP). Single threshold detection simplifies the electronics and presumably reduces the overall detector cost. Provided that light yield per MIP is adequate, extruded rather than expensive cast scintillators can be used to reduce project costs further.

3. Simulations

In order to realize the full potential of a future linear electron–positron collider, a detector must have a jet energy resolution of $\sigma(E)/E \cong 30\%/\sqrt{E}$ (E is in GeV) [2, 3]. Most modern analog sampling hadron calorimeters have a jet energy resolution of the order of $\sim 80\%/\sqrt{E}$. Energy-flow algorithms (EFAs) attempt to separate, in a jet, the energy clusters from charged hadrons from those that come from neutral electromagnetic and hadronic particles. The charged particle cluster energy is then substituted by the momentum measurement of the matched track. The photons are measured with high precision in the electromagnetic calorimeter. In principle therefore, the hadron calorimeter with a traditional single particle resolution of $50\%/\sqrt{E}$ is only required to measure the energy of neutral hadrons that, on average, carry just $\sim 11\%$

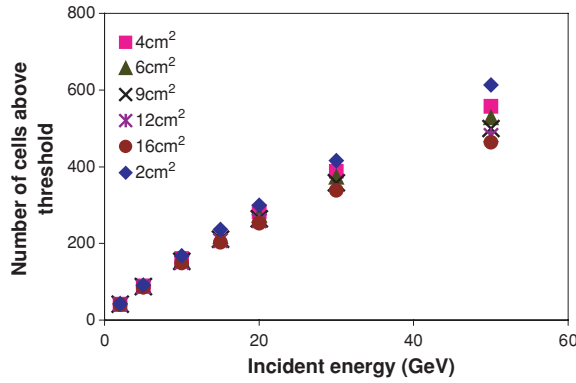


Figure 2. Number of hits above threshold (0.25 MIP) versus charged pion incident energy for various DHC cell sizes.

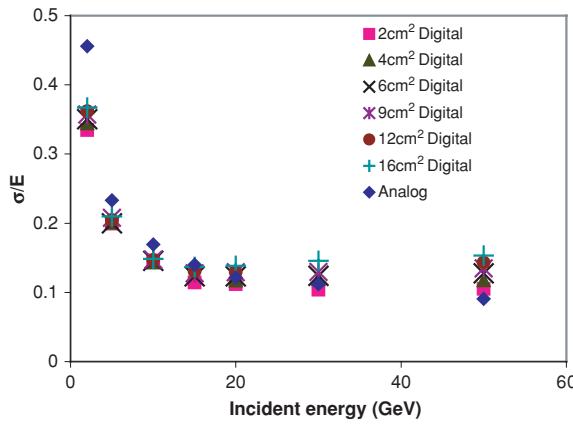


Figure 3. Energy resolution versus the incident energy of single charged pions.

of the jet's total energy. Thus, an LC detector, optimized for EFAs, could achieve a net jet energy resolution of $30\%/\sqrt{E}$. A highly segmented hadron calorimeter can make a significant contribution in achieving this performance by resolving closely spaced hadron showers.

A strong correlation between the number of hits and incident energy is required for a single threshold, or single bit, DHC to measure energy (figure 2). Figure 3 shows the energy resolution of single charged pions as a function of their incident energy, for a GEANT4 simulation of a scintillator sampling hadron calorimeter, instrumented with square cells of areas 2, 4, 6, 9, 12 and 16 cm². In any individual run, all cells of the calorimeter had the same area. The resolution curves indicate that the digital (where the number of cells is taken as the measure of the pions energy) and analog approaches give comparable performances in simulations. A cell is counted for the purposes of estimating the energy, if its response exceeds 0.25 times the energy that would be deposited by a minimum ionizing particle.

To evaluate the jet energy resolution in a quasi-algorithm-independent fashion, stable, generated MC particles were clustered into 0.7 simple cone jets. Constituent energies were smeared using the following prescription:

- (a) Charged particles were not smeared at all.
- (b) Photons were smeared with a $17\%/\sqrt{E}$ sampling term.

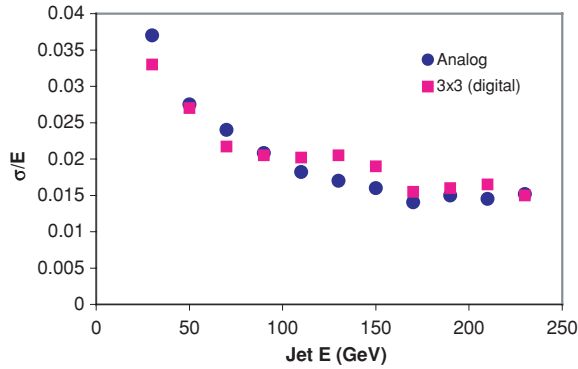


Figure 4. Energy resolution for jets in e^+e^- collisions at $\sqrt{s} = 500$ GeV.

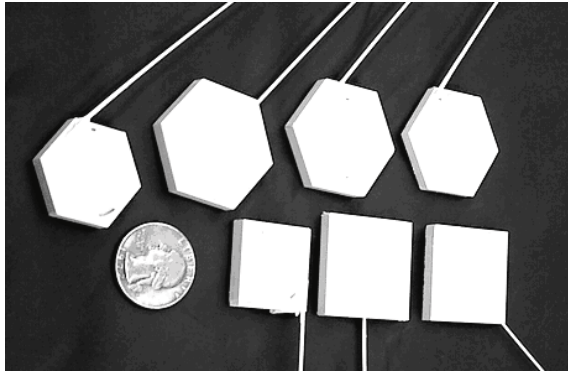


Figure 5. The different species of cells and grooves investigated in this study.

(c) Neutral hadrons were smeared using the fractional resolution shown in figure 3 for the $3 \times 3 \text{ cm}^2$ cells.

The energy of the jets with and without smearing is compared to obtain the parametrized jet energy resolution, as shown in figure 4. As can be seen from the figure, the ‘digital’ resolutions are competitive with analog resolutions even for high energy jets.

4. Prototyping the scintillating calorimeter

Instrumentation of a calorimeter with small scintillating cells presents unique challenges in terms of tile–fibre–photo-detector optimization and cell processing. We address some of these issues in the following studies. These prototyping studies were carried out using a large variety of fibres and scintillators (see appendix A). Wherever appropriate we indicate the materials and experimental setup used for any particular investigation.

4.1. Optical fibre bending

Since the WLS fibres need to be inserted into small scintillator cells (figure 5) as envisioned in our proposal, the response as a function of bending radii is a critical parameter.

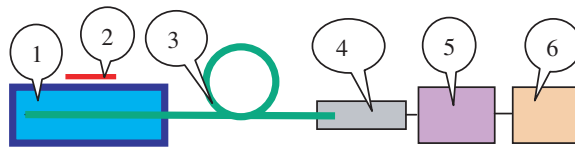


Figure 6. Schematic of the apparatus to measure the WLS response as a function of the bending diameter: 1 is a scintillating cell; 2 is a ^{90}Sr radioactive source; 3 is a circular fibre loop; 4 is a photomultiplier tube R-580;¹ 5 is a picoammeter² and 6 is a PC based data acquisition system.

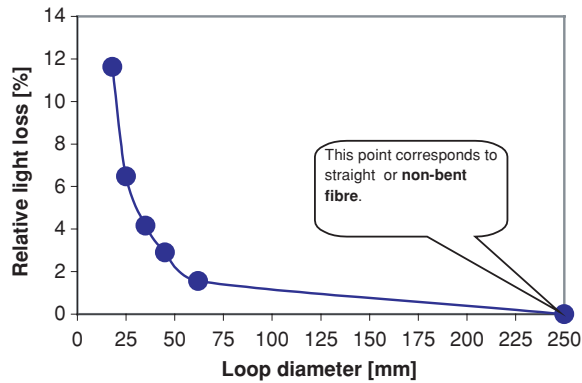


Figure 7. Light loss as a function of the bending diameter, for round 0.9 mm outer diameter BCF-92 fibre.

Table 1. Normalized response of cells for different kinds of surface treatments.

Surface treatment	Unpolished top and polished bottom	Polished top and polished bottom	Unpolished top and unpolished bottom
Response	0.98	1.00	1.02

Light loss from bending of the BCF-92, round, 0.9 mm diameter WLS fibre was measured using the light created in a scintillating cell with a ^{90}Sr radioactive source (figure 6).

The part of the fibre not embedded in the cell was manipulated into circular loops of varying radii. All parts of the fibre outside the loop were straight and fixed to the bench. The response was measured for different inner diameters of the loop. Straight fibre response was considered as zero bending loss. Figure 7 shows the light loss for different loop diameters. For loop diameters that are applicable to our 9 cm² cells, light losses due to bending are small (4–5%), giving us the freedom to use straight and curved grooves for our cells.

4.2. Cell surface treatment

To quantify the effect of cell surface machining on response, three sets of similar cells with polished or machined surfaces, either top or bottom, were tested. The results are summarized in table 1. The accuracy of measurement at each point was $\pm 2\%$. The average responses were virtually identical, so surface treatment of the top and bottom faces has no significant effect on

¹ Hamamatsu Corporation, 360 Foothill Road, PO Box 6910, Bridgewater, NJ 08807-0919, USA; 314-5, Shimokanzo, Toyooka-village, Iwata-gun, Shizuoka-ken, 438-0193 Japan.

² Keithley Instruments, Inc., 28775 Aurora Road, Cleveland, OH 44139, USA.

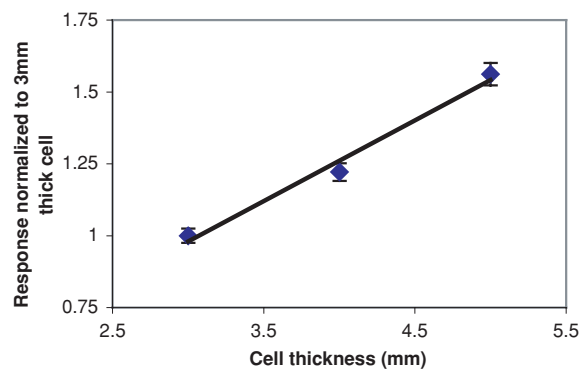


Figure 8. Response of cells with the thicknesses of 3, 4 and 5 mm.

the cell response, thus eliminating the need for the time and labour-intensive step of polishing. However, we did find an effect of surface treatment on the sides that is discussed in section 4.

4.3. Cell thickness

Cell response versus thickness was studied for cells of 3 to 5 mm thickness. The cells were hexagonal with an area of 9.4 cm^2 . Each cell had a WLS fibre inserted into a sigma-shaped groove. Since the thickness range was small, all cells were made from the same strip of cast scintillator, with an initial thickness of 5.5 mm (see section 4.2).

Response as a function of thickness is shown in figure 8, where each point represents the average response of eight cells. Units for response were normalized to the average response for 3 mm thick cells. A ^{137}Cs radioactive source was used. The response is a linear function of the cell thickness up to 5 mm. The accuracy of measurement at each point was $\pm 2\%$.

4.4. Wrapping and coating

Cell response as a function of surface treatment, such as coating or wrapping, was tested. Tyvek has been traditionally used to cover scintillating tiles. For millions of small cells painting is an attractive alternative, because it is less labour intensive than manually wrapping each cell. Also, paint has reflective properties that capture light inside the cell, reduce optical crosstalk between the cells and provide a reflective outer surface that can serve as a reference target for metrology.

The following geometry, materials and tools were used to test surface treatments:

1. Cells were made out of 5 mm thick BC-408 scintillator, with hexagonal shape and area of 9.4 cm^2 ; five out of 11 had polished edges.
2. The cell groove was sigma-shaped with a rectangular cross-section, 12 mm radius, 1 mm width, 4.5 mm depth and an angled exit. The groove itself makes an incomplete circle covering 335° . The groove for the WLS fibre must be angled; otherwise, the cells cannot be placed adjacent to each other without additional gaps (dead zones) between sides.
3. The WLS fibres were square BCF-92 with 0.9 mm sides, embedded and glued into the groove using BC600 optical glue.
4. Wrapping or coating materials were Tyvek, CM500, VM2002 and CM590 radiant light films from 3M,³ aluminized Mylar, titanium white acrylic paint from Liquitex⁴, and

³ 3M Light Management Ventures, 3M Center Building, 0223-01-N-12, St. Paul, MN 55144-1000, USA.

⁴ 2000 Liquitex Artist Materials, PO Box 246, Piscataway, NJ 08855, USA.

Table 2. Normalized cells response for different coating or wrapping.

Coating	Tyvek	Paint	VM2002	Mylar	CM590	CM500	Aluminium
Response	1.00	0.89	1.08	0.83	0.28	0.44	0.63

Table 3. Ratio of response for cells with unpolished sides to the response of cells with polished sides.

Coating	Tyvek	Paint	VM2002	Mylar	CM590	CM500
Ratio	1.27	1.30	1.28	1.30	1.14	1.19

Table 4. Normalized cell response for different coating materials.

Type of coating/wrapping	Relative response
Tyvek	1.00
Aluminized Mylar adhesive tape	0.48
Aluminium sputtering	0.24
Paint BC620	0.98
Paint white acrylic	0.90
Paint black acrylic	0.06

aluminium foil. Artists' titanium dioxide white acrylic paint from Liquitex was used for the tests described below since Saint-Gobain BC-620 reflective paint did not provide a solid finish, but instead resulted in the powdery surface that would wear away on contact.

5. A Hamamatsu (see footnote 1) R580 photo-multiplier tube operating at 1300 V was used. The dark current was less than 0.07 nA, or less than 0.1%, for regular ^{90}Sr (2 mCi) measurements. Current was measured with a Keithley picoammeter (see footnote 2) interfaced with a PC via GPIB.

Normalized cell responses for different coatings or wrappings are summarized in table 2. All measurements were made with the same cells that were consecutively wrapped in each material and then, finally, painted in white acrylic. Super-reflective film provided the best response. Painted cells had a response of 11% less than Tyvek-covered cells.

Response comparisons between coated or wrapped cells with polished versus non-polished sides are shown in table 3. The accuracy of averages for these measurements was 3%. For common coating or wrapping materials, cells with non-polished sides provided up to 30% larger response than cells with polished sides. For higher response, the cell treatment choice for the sides was more important than for surfaces.

We also measured the response of mirrored cells with the hope that such treatment could provide enough light, minimal dead zones and low optical crosstalk between cells. The response was compared with cells wrapped in Tyvek, painted with BC-620, wrapped in adhesive mirrored tape or painted in black ivory. The results are summarized in table 4. The mirrored cells provided, on average, four times less response than cells wrapped in Tyvek. The very low response of cells painted in black illustrates the importance of surface treatment.

Gaps between the cells' edges significantly reduce the array efficiency of particle registration. Therefore, the thickness of paint should be small. On the other hand, if the thickness of the paint is insufficient, the cell response will be reduced and the optical crosstalk between the cells will be high. Thus, the thickness of the paint must be optimized. If the



Figure 9. NICADD prototype of a scintillating digital hadron calorimeter. In the top left corner a photograph of a cell array is shown.

white-acrylic paint thickness was more than 0.2 mm, the optical crosstalk to adjacent neighbours was negligible, as discussed in the next section.

4.5. Optical crosstalk between cells

Optical crosstalk, or ‘light leaks’ between cells, occurs when light penetrates from one cell to another through the sides. If the level of optical crosstalk is higher than the electronic threshold, it will be detected as a particle. This kind of noise can confuse the event reconstruction process. The measurement described below shows that the crosstalk between the adjacent cells is less than 1%.


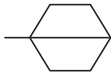
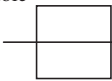
The optical crosstalk from the central cell to its six neighbours (the arrangement of cells was identical to the one shown in the top left corner of figure 9) was measured using an array of seven hexagonal cells. A 5 mCi ^{90}Sr radioactive source was used to generate light in the central cell. These measurements were performed using a Hamamatsu PMT R-580 instrumented with an optical mixer. The WLS fibres from all cells were connected to the PMT via square plastic ferrules with 4.2 mm sides. The mixer reduces the non-uniformity across the PMT photocathode to less than 0.1%. The current measurements were performed using a Keithley picoammeter. The accuracy of these measurements was 0.5%.

The measurements were first performed with all seven cells connected to the PMT and the radioactive source positioned in the middle of the central one. All subsequent measurements were normalized with respect to the current response obtained for this measurement. Next, the neighbouring cells were disconnected from the PMT and the response of the central cell alone was measured. The response obtained in this configuration is 1.5% less than when all the seven cells were connected to the PMT. Even though this is already acceptable, the 1.5% should not be interpreted as the level of crosstalk since the measurements were made with a source

Table 5. Normalized response measured for cells of different shapes and areas.

Shape and area	Hexagon 9.4 cm ²	Square 9.4 cm ²	Hexagon 6.0 cm ²	Square 6.0 cm ²	Square 4.0 cm ²
Response	1.00	0.95	0.93	0.93	0.85

Table 6. Normalized response of cells with different shapes and grooves.

Cell shape	Hexagon	Hexagon	Square
Groove for WLS fibre	Sigma 	From corner to corner extruded hole 	From side to side extruded hole 
Response	1.00 ± 0.02	0.89 ± 0.02	0.85 ± 0.03
Uniformity	Uniform	Non uniform	Non uniform

that will cause leakage of particles into cells surrounding the central cell. To estimate this effect we measure the response of the six neighbours with the central cell wrapped in Tedlar and disconnected from the PMT. The Tedlar wrapping eliminates the optical crosstalk from the central cell to its neighbours, and the response obtained for the neighbours will therefore reflect the amount of light generated by the source in them. On measurement this contribution was measured to be 0.6%, which needs to be subtracted from the previously obtained 1.5% to get the correct estimate of the crosstalk level $\sim 0.9\%$. The net crosstalk level per cell per side ($\sim 0.13\%$) is therefore negligible.

4.6. Cell shape, area and groove

Most cell responses as a function of shape and area were measured with hexagonal and square cells with angled sigma grooves of 1.2 mm width for the WLS fibres and areas of 9.4 and 6.0 cm². In addition, cells with 4.0 cm² area with a straight angled groove were made. The angled groove starts at a depth of 4.5 mm and becomes progressively shallower to 0 mm at the exit. Eight cells were used for each measurement. The measurement accuracy was $\pm 2\%$. The results are given in table 5.

The comparison shows that cell responses are only moderately sensitive to the cell's area or shape. No cracks in WLS fibres were detected, even in the smallest cells (6 cm² area) with sigma groove. We also measured the response of hexagonal cells made from extruded NICADD/FNAL scintillator with sigma grooves. The extruded scintillator had a response $60 \pm 0.02\%$ that of the cast scintillator [6, 7].

The effect of groove type was also tested for a straight groove, sigma-shaped angled groove and round, extruded hole with embedded and glued WLS fibres. The results for 9.4 cm² cells are shown in table 6. All these measurements used the NICADD-FNAL extruded scintillator with 4.87 mm thickness. A ⁹⁰Sr radioactive source was placed in the centre of the cells. The data are normalized to the average response of a hexagonal cell with an angled sigma groove.

Table 7. Measurements of spatial uniformity.

Cell shape and WLS fibre groove type	Figure
Hexagonal with extruded hole	A1
Square with extruded hole	A2
Square with angled sigma groove	A3
Hexagonal with angled sigma groove	A4
Square with straight angled groove	A5
Two hexagonal cells with sigma groove	A6

4.7. Uniformity of the response across a cell

The uniformity of cell response with straight or sigma grooves was measured. The cell shape, together with the shape of the groove, define the unique response to a charged particle. A mapping of the cell response provides information for choosing the electronic threshold and comparing cell designs. The scanned cells had the same area (9.4 cm^2) and thickness (5 mm). A ^{90}Sr radioactive source with a 2 mm collimated slit was used for these measurements. The accuracy of the source positioning was 0.2 mm. For uniformity measurements, the cell was flipped, levelled and put on a soft surface to protect the WLS fibre. The collimated source was moved along the bottom surface of the cell. The tests are enumerated in table 7 and detailed plots are presented in appendix B.

4.8. Light loss in the cell due to aging

To examine light yield of a cell as a function of time, the response measurement was repeated 4–6 months after production. The measurements were made with 30, 9.4 cm^2 hexagonally shaped cells with Kuraray 1 mm diameter, Y-11, multiclاد, S-type WLS fibres glued inside the angled sigma groove. Within the margin of error, the response was stable over the entire period. The average after 6 months was 0.993 ± 0.006 of the original response at the time of production.

4.9. DHC prototype

Based on our tile–fibre optimization studies, we have assembled a scintillating digital hadron calorimeter (SDHC) prototype shown in figure 9. It consists of the following major components: scintillating cells, optical fibres, photo-detectors and passive material. The prototype is a stack of 12 active layers, each consisting of an array of seven identical 9.4 cm^2 hexagonal cells (figure 9). Each cell has dimensions close to the effective Moliere radius [4] of the brass-scintillator sandwich. The arrays are readout with six Hamamatsu H8711 assemblies (see footnote 1) (multi-anode photomultiplier tube (MPMT) with 16 channels) via 1 m long WLS fibres connected to clear fibres with optical connectors. Each passive layer is a $125 \times 125 \times 25 \text{ mm}^3$ brass plate. The prototype was tested with cosmic rays.

The prototype shown in figure 9 was read out using a trigger to select particles with tracks along the stack. The system used a V792N series QDC from CAEN⁵ and a LabVIEW-based DAQ system. Figure 10 shows the response for a MIP [8]. The peak between the pedestal and ~ 115 QDC channel is due to the crosstalk from adjacent channels inside the MPMT.

Figure 11 shows the response of the same MPMT channel to the light-emitting diode (LED) signals that were significantly attenuated with grey optical filters in order to obtain a

⁵ CAEN, in USA—WIENER Plein & Baus Corp., 300 East Auburn Ave., Springfield, OH 45505.

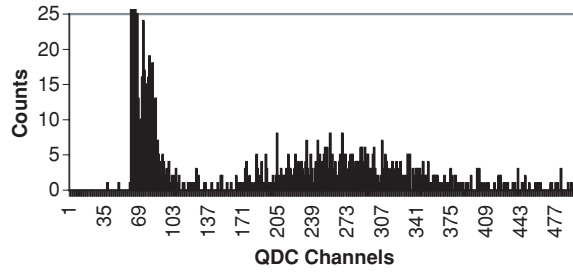


Figure 10. Cell and MPMT H8711 response to a MIP.

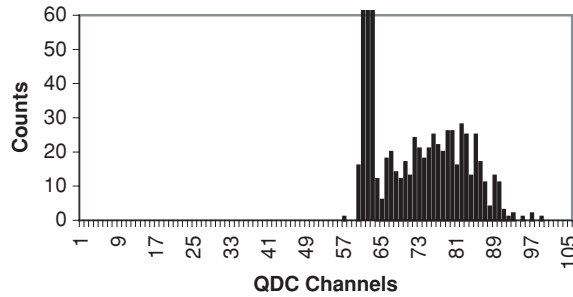


Figure 11. Single electron spectrum for H8711. LED signal was attenuated with grey optical filters.

single electron spectrum. The analysis of these plots shows that the MPMT peak in figure 10 corresponds to ~ 12 photoelectrons per MIP per cell [9].

4.10. Photo-detectors

The operation of the DHC within a strong magnetic field, essential for the EFAs, excludes the use of standard photomultiplier tubes. New solid-state photo-detectors, such as the SiPM ('Pulsar' Enterprise [10], Russia) or the MRS ('CPTA' [11], Russia), are an attractive option. These devices have high gain ($5 \times 10^5 - 10^6$), low quantum efficiencies ($\sim 15\%$) and thus offer PMT-like performance. They are, however, immune to magnetic fields. Additionally, these photo-detectors can be inserted onboard the scintillator due to their small ($\sim 1 \text{ mm}^2$) size, thereby eliminating the need for routing fibres over long distances. Currently we are undertaking a detailed study of both of these promising candidates.

5. Conclusions and outlook

Simulations show that a scintillator-based digital hadron calorimeter can provide performance comparable to a fully analog calorimeter. In addition, the small scintillating cells provide better imaging capabilities for full event reconstruction.

Small scintillating cells with optical readout, needed for an HCAL, were studied with radioactive sources and cosmic rays. Based on our studies, a nominal cell element with $\sim 9 \text{ cm}^2$ area, hexagonal or square shape, angled sigma groove, and KURARAY, Y-11, multicladd, S-type, 1 mm diameter WLS fibre readout would meet the requirements of a DHC. Using PMTs (or SiPMs), these cells provide > 10 photoelectrons per MIP (measured with cosmic rays).

Further R&D will be needed in the following areas: production, assembly, choice of photo-detector and electronics and optimization of cell area. We plan to construct a test beam prototype and continue studies of the energy flow algorithms.

Acknowledgments

The authors are grateful to Peter Torres and Daniel Ruggiero for their help during the cell tests. We would also like to thank Phillip Stone for providing excellent mechanical and machining support. This work was supported in part by the U.S. Department of Education under grant no P116Z010035, the Department of Energy and the State of Illinois Higher Education Cooperation Act.

Appendix A

The following optical fibres were tested for the readout:

- Saint-Gobain⁶ BCF-92, square, 0.9 mm;
- Saint-Gobain BCF-92, round, 0.9 mm outer diameter (OD);
- Saint-Gobain BCF-92, round, 1.0 mm OD;
- KURARAY⁷, Y-11, S type, round, 0.94 mm OD, multiclاد;
- KURARAY, clear, S type, round, 0.94 mm OD, multiclاد;
- KURARAY, Y-11, S type, round, 1.00 mm OD, multiclاد.

All fibre ends were polished using the fly diamond cutting technique, and one end of each WLS fibre was aluminium- mirrored. All fibres were 1 m long. At least 100 samples of each type were tested.

The following materials were used to fabricate scintillating cells:

- Saint-Gobain (see footnote 6) BC-408; 5, 10 and 20 mm thickness;
- Eljen Technologies⁸ EJ-200; 3, 4 and 5 mm thickness;
- NICADD-Fermilab extruded [6], 5 mm thickness.

Appendix B

Figures A1(b) and (c) present the normalized uniformity response for a hexagonal cell. The cell with 38 mm length, 32 mm width and 9.4 cm² area was made from an extruded scintillating strip [6] with a co-extruded oval hole (2.1–2.8 mm diameter) in which a WLS fibre was inserted. Scans were performed along and across the WLS fibre embedded in the cell as shown by the dashed lines in figure A1(a).

Figures A2(b) and (c) present the normalized uniformity response for a square cell. The 9.4 cm² cell was made from extruded scintillating strip [6] with a co-extruded inside hole (2.1–2.8 mm diameter) in which the WLS fibre was inserted.

Figure A3(b) presents the normalized uniformity response for a square cell. The cell was made from cast scintillator (see footnote 8) with angled, 1.2 mm wide sigma groove for the WLS fibre.

⁶ Saint-Gobain (Bicron), 12345 Kinsman Road, Newbury, OH 44065, USA.

⁷ Kuraray America Inc., 200 Park Ave, NY 10166, USA; 3-1-6, Nihonbashi, Chuo-Ku, Tokyo 103-8254, Japan.

⁸ Eljen Technology, PO Box 870, 300 Crane Street, Sweetwater, TX 79556, USA.

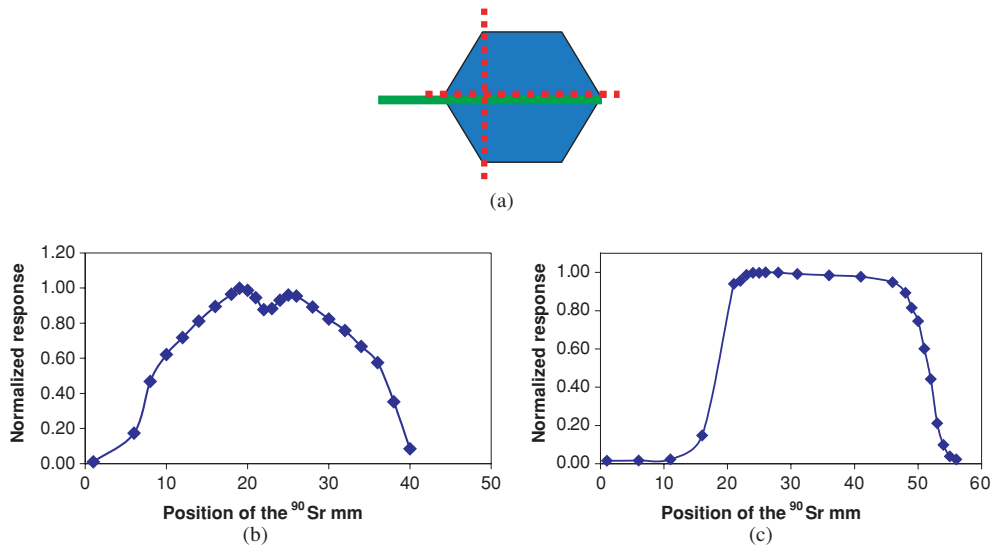


Figure A1. (a) A schematic of the hexagonal cell with WLS fibre (the solid line) embedded and glued inside an extruded hole. Dashed lines represent the scan directions. (b) A normalized response scan, performed across the fibre of a hexagonally shaped cell. The response was symmetric and up to 40% non-uniform near the edges. (c) A normalized response scan made along the fibre of a hexagonally shaped cell. The response was uniform with a small decrease at the mirrored fibre end.

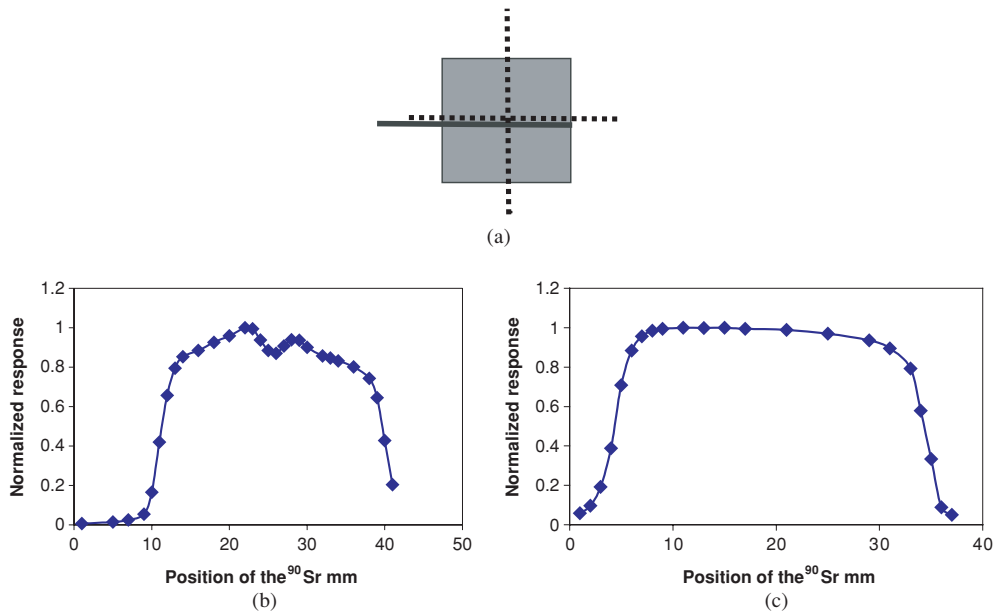


Figure A2. (a) A schematic of the square cell with WLS fibre (the black line) embedded and glued inside the extruded hole. The dashed lines represent scanning paths. (b) A normalized response for a scan performed across the fibre of a square-shaped cell. The response is up to 20% non-uniform at the edges. (c) A normalized response for a scan made along the fibre of the square-shaped cell. The response is uniform with a small slope near the mirrored end of the fibre.

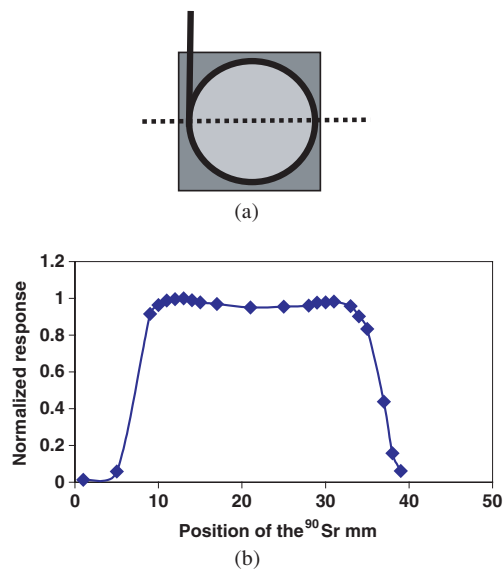


Figure A3. (a) A schematic of the square cell with WLS fibre (the black line) embedded and glued inside the angled sigma groove. The minimum distance between the edge of cell and the sigma groove is 1 mm. 30% of the cell area (darker in the picture) is out of the area enclosed by the sigma groove. (b) A normalized response scan, performed across a square-shaped cell with the angled sigma groove for WLS fibre. The response is uniform to within 5%.

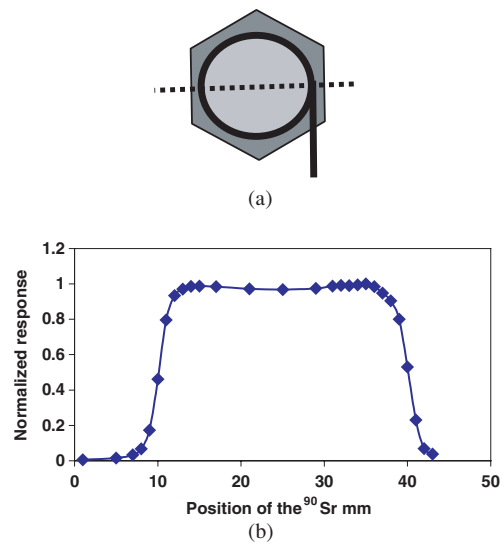


Figure A4. (a) A schematic of the hexagonally shaped cell with WLS fibre embedded and glued inside the angled sigma groove (the black line). The minimum distance between the edge of cell and the sigma groove is 1 mm. 20% of the cell area is not enclosed by the sigma groove (darker area in the picture). (b) A normalized response scan, performed across the hexagonally shaped cell with a angled sigma groove for WLS fibre. The response is uniform to within 3%.

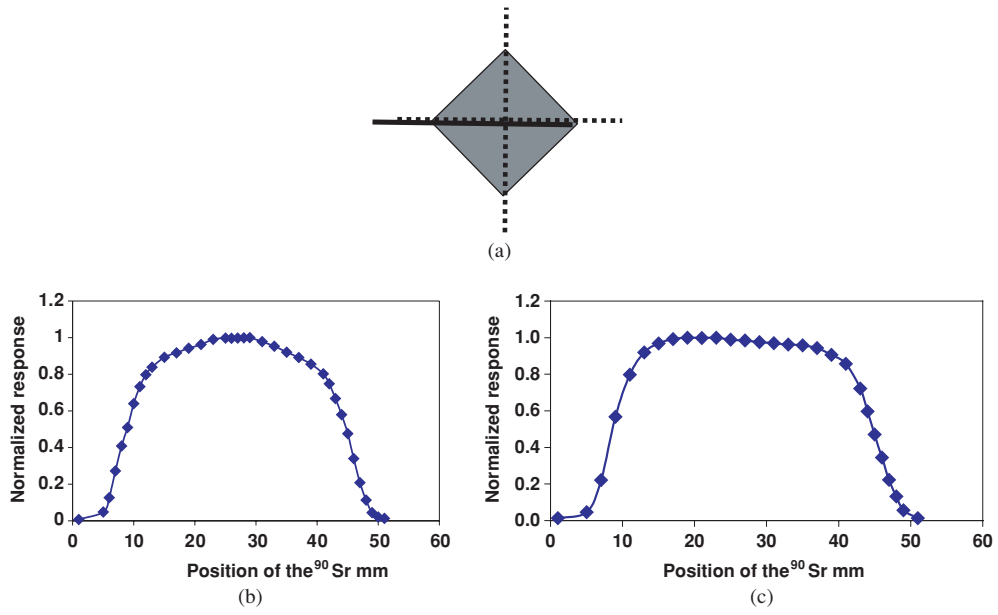


Figure A5. (a) A schematic of the square cell with WLS fibre (the black line) embedded and glued inside the angled straight groove. Dashed lines represent scan directions. (b) A normalized response scan, performed across the WLS fibre. (c) A normalized response scan, performed along the WLS fibre for the square cell.

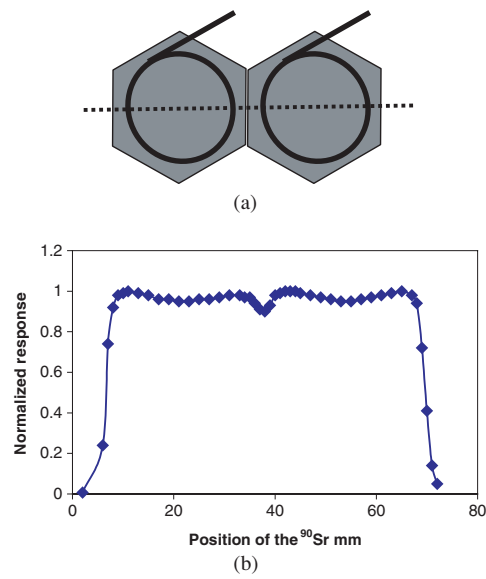


Figure A6. (a) A schematic of the hexagonally shaped cells with WLS fibre (the black line) embedded and glued inside the sigma grooves. Dashed line represents the scan direction. (b) A normalized response scan, performed across the hexagonally shaped cells with sigma grooves for the WLS fibre readout. The curve represents the summed response of two cells.

Figure A4(b) presents the normalized uniformity response for the hexagonally shaped cell shown in figure A4(a). The cell was made from cast scintillator (see footnote 8) with a 1.2 mm wide angled sigma groove for the WLS fibre.

Figures A5(b)–(c) present the normalized uniformity response for a square cell. The cell was made from cast scintillator (see footnote 8) with 1.2 mm wide angled straight groove for the WLS fibre.

Figures A6(b) presents the normalized uniformity response for two hexagonally shaped cells with WLS fibres connected to the same photomultiplier tube.

References

- [1] Damerell C *et al* 1996 *Proc. Snowmass* p 431
Brau J *et al* 1996 *Proc. Snowmass* p 437
Jaros J 2003 Silicon detector tracking *ALCPG Workshop Cornell (15 July)*
- [2] Lobban O *et al* 2002 On the energy measurement of hadron jets *Proc. 10th Int. Conf. on Calorimetry in Particle Physics (Pasadena)* (Singapore: World Scientific) pp 814–33
- [3] *TESLA Technical Design Report* DESY, March 2001
- [4] Morgunov V 2002 Calorimetry design with energy-flow concept (Imergin detector for high energy physics) *Proc. 10th Int. Conf. on Calorimetry in Particle Physics (Pasadena)* (Singapore: World Scientific) pp 70–84
- [5] CMS 1997 *The Hadron Calorimeter Project Technical Design Report* CERN/LHCC 97cmS TDR 2
- [6] Pla-Dalmau Anna, Bross Alan D and Rykalin Victor V 2003 *Extruding Plastic Scintillator at Fermilab* FERMILAB-Conf-03-318-E
- [7] *The MINOS Detectors Technical Design Report* NuMI-L-603, 1 March 1999
- [8] Francis K 2004 Evaluating small scintillating cells for digital hadron calorimeter *Master's Thesis*, NIU, DeKalb, IL (unpublished)
- [9] Bross A *et al* 2003 The digital hadron calorimeter (DHC) elements test, FERMILAB-TN-733
- [10] Bondarenko G *et al* 2000 *Nucl. Instrum. Methods A* **242** 187
- [11] Golovin V *et al* 1998 Limited geiger-mode silicone photodiode with very high gain *Nucl. Phys. Proc. Suppl. B* **61** 347–52